

Kinematics of SiO $J=8-7$ Emission towards the HH 212 Jet

Michihiro TAKAMI¹, Shigehisa TAKAKUWA², Munetake MOMOSE³, Masa HAYASHI¹,
Christopher J. DAVIS⁴, Tae-Soo PYO¹, Takayuki NISHIKAWA¹, and Kotaro KOHNO,⁵

¹*Subaru Telescope, 650 North A'ohoku Place, Hilo, Hawaii 96720, USA*

²*National Astronomical Observatory of Japan, Osawa, Mitaka, Tokyo 181-8588, Japan*

³*Institute of Astronomy and Planetary Science, Ibaraki University, Bunkyo 2-1-1, Mito, Ibaraki 310-8512, Japan*

⁴*Joint Astronomy Centre, 660 North A'ohoku Place, University Park, Hilo, Hawaii 96720, USA*

⁵*Institute of Astronomy, The University of Tokyo, 2-21-1 Osawa, Mitaka, Tokyo 181-0015*

(Received 2006 January 0; accepted 2006 0)

Abstract

We present SiO $J=8-7$ (347.3 GHz) observations towards HH 212 using the ASTE telescope. Our observations with a 22''-diameter beam show that the SiO emission is highly concentrated within 1' of the driving source. We carefully compare the SiO observations with archival H₂ 1-0 S(1) images and published H₂ echelle spectra. We find that, although the SiO velocities closely match the radial velocities seen in H₂, the distribution of H₂ and SiO emission differ markedly. We attribute the latter to the different excitation conditions required for H₂ and SiO emission, particularly the higher critical density ($n_{H_2} \sim 10^8 \text{ cm}^{-3}$) of the SiO $J=8-7$ emission. The kinematic similarities imply that the H₂ and SiO are associated with the same internal working surfaces. We conclude that the SiO $J=8-7$ emission has a potential to probe the jet/wind launching region through interferometric observations in the future, particularly for the youngest, most deeply embedded protostars where IR observations are not possible.

Key words: ISM: jets and outflows — ISM: kinematics and dynamics — line: formation

1. Introduction

Jets/outflows are a key phenomenon for the evolution of young stellar objects (YSOs). Theories predict that these outflows remove excess angular momentum from the accreting material, thereby allowing mass accretion to occur (see e.g., Shu et al. 2000; Königl et al. 2000). Observing the kinematics in the flow acceleration region is important if we are to understand this physical link. Unfortunately, there are two crucial problems which hinder the investigation through this approach. One is the limited spatial resolution of telescopes: these are in most cases insufficient to fully resolve the jet/wind launching region, which is believed to be located within a few AU of the driving source. The other is the fact that such a region is often deeply embedded within a massive envelope, making it difficult to observe at optical to near-IR wavelengths.

The rotation of jets/winds is arguably easier to observe than the kinematics in their launching regions. Such observations are therefore useful for the understanding the mechanism of mass ejection and accretion. Several observations have been attempted at optical-IR wavelengths, providing results consistent with the magneto-centrifugal wind scenario (see, e.g., Davis et al. 2000; Bacciotti et al. 2002; Coffey et al. 2004; Woitas et al. 2004). However, this approach may be hampered by spurious wavelength shifts of the grating spectrographs, or the interaction of the jet with the inhomogeneous ambient medium (cf. Bacciotti et al. 2002).

Millimeter/sub-millimeter interferometry in the near future has a great potential to overcome these difficulties for

studying kinematics in the jet/wind launching region, and also measuring flow rotation. We have therefore begun to search for appropriate emission lines for these studies using the ASTE (Atacama Submillimeter Telescope Experiment) telescope, a single-dish 10-m submillimeter telescope in northern Chile. ASTE is a pioneering activity on submillimeter astronomy at the ALMA site (Ezawa et al. 2004). In this paper we present SiO $J=8-7$ (347.3 GHz) observations towards HH 212. SiO emission at mm-submm wavelengths has been observed towards a number of outflows associated with low-mass YSOs (see e.g., Mikami et al. 1992; Codella, Bachiller & Reipurth 1999; Hirano et al. 2001; Nisini et al. 2002, 2005; Gibb et al. 2004). The emission associated with these objects is likely to originate in shocks via grain sputtering or grain-grain collisions releasing Si-bearing material into the gas phase (e.g., Schilke et al. 1997; Caselli, Harquist & Havenes 1997; Pineau des Forêts et al. 1997). The observations to date have revealed that the kinematics in SiO emission markedly differ from millimeter CO emission, a well-known probe of molecular bipolar outflows (e.g., Hirano et al. 2006; Palau et al. 2006). HH 212 is a highly symmetric two-sided jet in the Orion molecular cloud (Zinnecker, McCaughrean & Rayner 1998), lying within 5° of the plane of the sky (Claussen et al. 1998). Interferometric observations of millimeter CO/SO emission have been conducted by Lee et al. (2000, 2006) with an angular resolution down to a few arcsecond, revealing the origins of these lines.

In this paper we show that the SiO $J=8-7$ line in this object is probably associated with the ejecta of the col-

limited jet, in particular its internal working surfaces. Due to this fact, together with its high critical density ($n_{H_2} \sim 10^8 \text{ cm}^{-3}$), this line has a potential to probe the jet/wind launching region through interferometric observations in the future.

2. Observations and Results

Observations were made using the ASTE telescope on August 27–28 2005. The antenna diameter of 10-m provides a FWHM beam size of $22''$ at 350 GHz, corresponding to 0.05 pc at a distance of 450 pc. The telescope is equipped with an SIS heterodyne-receiver and an XF-type digital auto-correlator that gives a 0.5 MHz frequency resolution over the total bandwidth of 512 MHz. The weather was quite good, with a system temperature of 180–260 K. The pointing was checked every few hours and was found to be accurate to better than $3''$. OMC-1 was also observed for calibration with standard spectra. Performing comparisons with the data obtained at the CSO 10.4-m telescope (Schilke et al. 1997), we derive the main beam efficiency $\eta_{MB}=0.73\text{--}0.74$ during the observations.

The spectra were obtained towards three well-known low-mass outflow sources, including a Class 0 protostar (HH 212) and two Class I protostars (SVS 13 and L1551-IRS 5), with an initial resolution of 0.5 MHz. All of these objects exhibit bright H_2 emission due to shocks (e.g., Davis et al. 1995, 2000, 2002, 2006). In HH 212 and SVS 13, seven and two points were observed along the jet, respectively. Each spectrum was binned to increase signal-to-noise, providing a velocity resolution of 4.3 km s^{-1} . The results are summarized in Table 1. We detect the emission clearly at the driving source and $20''$ north/south, and marginally at $40''$ north/south in HH 212. Upper limits to the brightness temperature of 0.02–0.03 K are obtained for the remaining two positions and for the other two targets. The non-detection towards the two Class I protostars corroborate previous SiO $J=5\text{--}4$ observations, which show that SiO emission is preferentially detected towards Class 0 protostars (Gibb et al. 2004).

Figure 1 shows the position and line profiles observed towards HH 212. The line profile at $20''$ north shows only a blueshifted component, while that at $20''$ south shows only a redshifted component. The line profiles observed at $20''$ north and south peak at -8 and 5 km s^{-1} , respectively: i.e., $\sim 10 \text{ km s}^{-1}$ blueshifted and $\sim 3 \text{ km s}^{-1}$ redshifted with respect to the systemic velocity of the cloud core (1.6 km s^{-1} , Wiseman et al. 2001). These flow velocities are markedly larger than those observed in CO $J=1\text{--}0$ emission, whose peaks are only $1\text{--}2 \text{ km s}^{-1}$ blueshifted/redshifted (see Lee et al. 2000).

Davis et al. (2000) obtained three adjacent, parallel long-slit spectra of H_2 1-0 S(1) emission ($2.122 \mu\text{m}$) along the axis of the HH 212 jet, with a $0.5''$ separation between the slits. To perform comparisons of kinematics between the H_2 and SiO emission, we summed these three spectral images and plot H_2 profiles in Figure 2 for individual emission knots. The SiO profiles at the adjacent positions are also shown. The figure shows that the velocity observed in

Table 2. H_2 1-0 S(1) Peak and FWHM velocities

Knot	Offset ^a (arcsec)	Peak V_{LSR} ^b (km s^{-1})	V_{FWHM}	
			observed (km s^{-1})	deconvolved ^c (km s^{-1})
NB 1/2	39	-12	31	24
NK 7	24	-8	21	9
NK 4	13	-8	20	6
NK 2	10	-8	23	12
NK 1	5	-4	36	31
SK 1	-6	5	28	21
SK 2	-10	7	20	6
SK 4	-14	10	19	—
SB 1/2	-40	10	25	16

^aBased on Zinnecker et al. (1998).

^bThe uncertainty is $\pm 2 \text{ km s}^{-1}$.

^cAssuming $v_{obs}^2 = v_{dec}^2 + v_{ins}^2$, where v_{obs} , v_{dec} and v_{ins} are the FWHM velocity of the observed, deconvolved and instrumental profiles, respectively.

the SiO emission is very similar to that of the H_2 emission. Indeed, the northern H_2 knots and bow shock, NK 1–7 and NB 1/2, exhibit a peak velocity of -4 to -12 km s^{-1} , matching well with the SiO peak velocity observed at $20''$ north of the driving source (-8 km s^{-1}). The southern knots and bow shock (SK 1–4 and SB 1/2) exhibit a peak velocity of $5\text{--}10 \text{ km s}^{-1}$. The H_2 peak velocity at SK 1 coincides with the SiO peak velocity, whereas the H_2 peak velocity observed in the other structures are slightly larger than the SiO peak velocity. The H_2 profiles at NK 2–7 and SK 3–4 shows FWHM velocities of $19\text{--}23 \text{ km s}^{-1}$, significantly larger than the SiO emission at the corresponding beam ($10\text{--}15 \text{ km s}^{-1}$ at $20''$ north/south). Note, however, that this is due to the instrumental broadening of the H_2 profiles (19 km s^{-1}). We derive the deconvolved FWHM velocities to be less than 15 km s^{-1} for NK 2–7 and SK 3–4 assuming $v_{obs}^2 = v_{dec}^2 + v_{ins}^2$, where v_{obs} , v_{dec} and v_{ins} are the FWHM velocity of the observed, deconvolved and instrumental profiles, respectively. The H_2 1-0 S(1) peak and FWHM velocities for the individual knots are tabulated in Table 2

Although the H_2 and SiO velocities are closely correlated, their distributions differ markedly. The SiO $J=8\text{--}7$ flux is highly concentrated within $1'$ of the driving source. This contrasts with the distribution of the H_2 1-0 S(1) and CO $J=1\text{--}0$ emission, which extend over a minute along the jet axis (see Figure 1; Lee et al. 2000). The strongest SiO emission coincides with regions where H_2 knots are relatively faint ($20''$ north and south of the source), while the brightest H_2 knots NB 1/2 and SB 1/2 correspond with weaker SiO emission. To show this quantitatively, we reduced narrow-band H_2 images obtained using VLT-ISAAC on October 19 and November 7 2003, and analyzed the images as follows. After sky-subtraction and flat-fielding, the flux from the foreground/background stars were carefully removed, then the H_2 flux above the 5-sigma level (corresponding to 2% of the peak flux at SK 2) was measured in each gaussian beam with a FWHM of

Table 1. SiO $J=8-7$ Brightness Temperatures and Integrated Intensities

Object	R.A. (2000)	Dec. (2000)	Jet P.A. ^a (deg.)	Offset (arcsec)	Peak T_{MB} (K)	$\int T_{MB} dv$ (K km s ⁻¹)
HH 212	5 ^h 43 ^m 51.0 ^s	-01°02'52"	22	+60	<0.02	— ^b
				+40	0.06±0.02	— ^b
				+20	0.22±0.03	2.98±0.07
				0	0.19±0.02	3.81±0.04
				-20	0.21±0.03	2.26±0.04
				-40	0.06±0.02	— ^b
SVS 13	3 ^h 29 ^m 03.7 ^s	+31°16'04"	123	0	<0.02	—
				+20	<0.02	—
L1551-IRS 5	4 ^h 31 ^m 31.3 ^s	+18°08'05"	—	0	<0.02	—

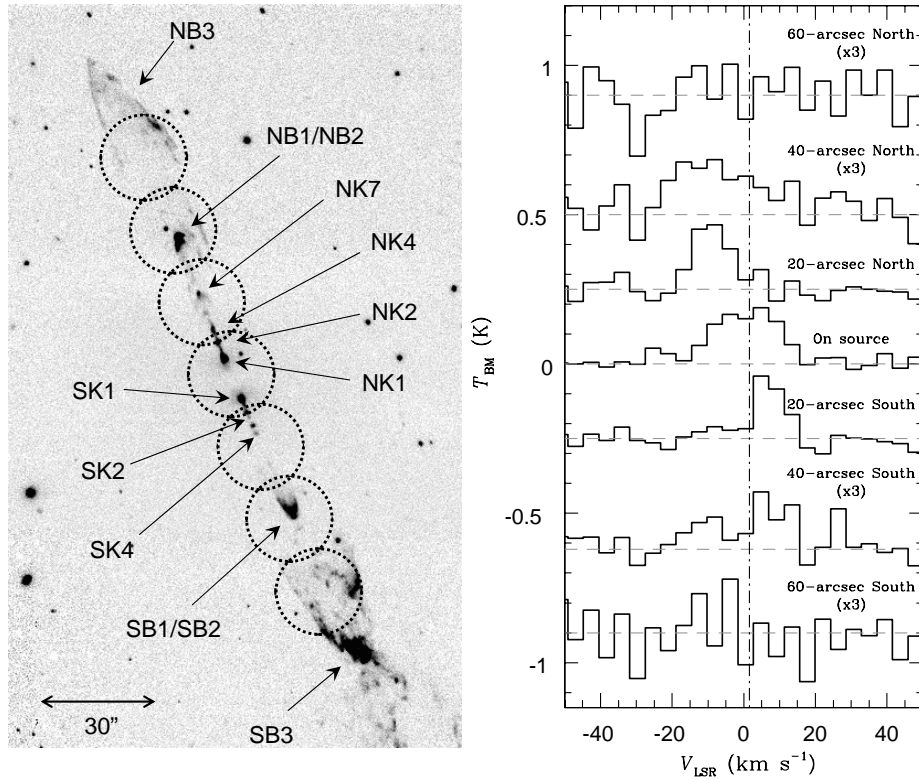
^aDavis et al. (2000)^bWe cannot measure the integrated intensity since the signal-to-noise is not sufficient for determining the velocity range.

Fig. 1. (left) Narrow-band H₂ 1-0 S(1) (2.122 μ m) image of HH 212 obtained using VLT-ISAAC. The raw images were obtained from the ESO Archive. The name of the knots are based on Zinnecker et al. (1998). Dotted circles indicate the positions and beam size (22'') of the ASTE observations. (right) SiO $J=8-7$ line profiles observed at seven positions. The brightness temperature at 40–60'' north/south is multiplied by 3 to emphasize marginal features. The dot-dashed line indicates the systemic velocity of the molecular core ($V_{LSR}=1.6$ km s⁻¹, Wiseman et al. 2001)

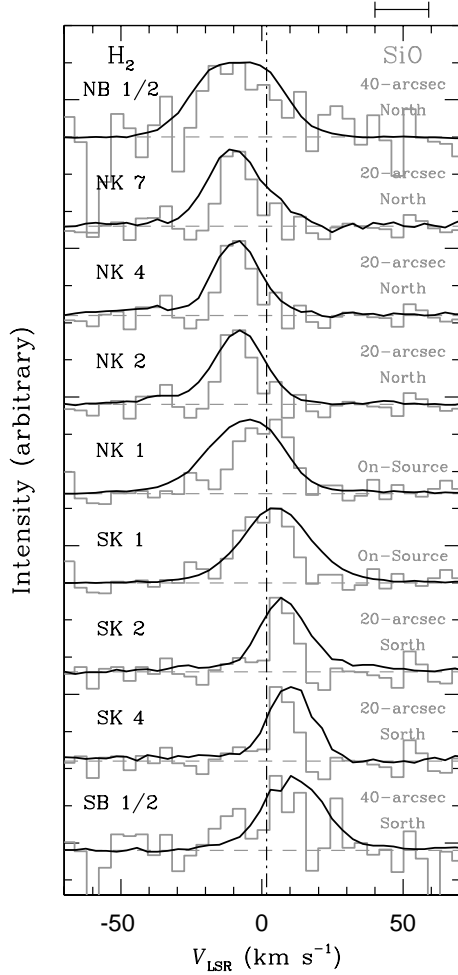


Fig. 2. H_2 1-0 S(1) line profiles observed at each knot (solid), together with the SiO $J=8-7$ profiles (histogram). Each knot is covered by the SiO beam as follows: NB 1/2 by the 40'' north beam; NK 2-7 by the 20'' north beam; NK 1 and SK 1 by the on-source beam; SK 2-4 by the 20'' south beam; and SB 1/2 by the 40'' south beam. The bar above the figure shows the FWHM of the instrumental broadening for the H_2 emission. The dot-dashed line indicates the systemic velocity.

22''. Figure 3 shows the intensity distribution of H_2 emission obtained in this way. The distribution of the SiO $J=8-7$ integrated intensity is also shown. The H_2 flux distribution shows flux minima at 20'' north and south, and the flux is greater at 40'' north and south by a factor of ~ 2 . The H_2 flux at 60'' south is comparable to that at the driving source. In contrast, the SiO emission is detected at 40'' north/south only marginally ($\sim 3\text{-}\sigma$), and not detected at 60'' north/south. Although the integrated intensity at these regions are uncertain, due to the uncertainty of the line profile, the brightness temperature suggests that the intensity at 40''-60'' north/south is smaller than the inner region by a factor of at least 3¹.

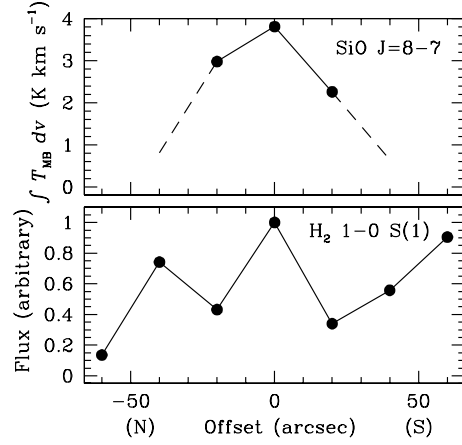


Fig. 3. Intensity distribution of SiO $J=8-7$ and H_2 1-0 S(1) emission measured using the same size apertures. Uncertainties are comparable or smaller than the filled circles.

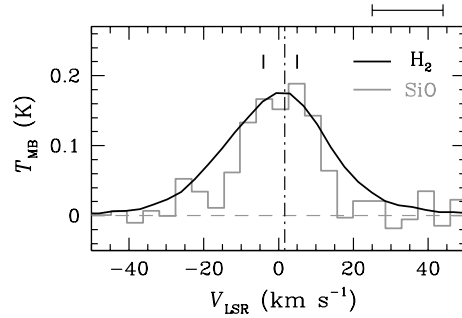


Fig. 4. The H_2 1-0 S(1) profile averaged from NK 1 and SK 1 (solid), and the SiO $J=8-7$ profile at the driving source (histogram). The marks at the top of the line profiles indicate the peak velocity for NK 1 and SK 1. The dot-dashed line indicates the systemic velocity of the molecular core. The bar at the top-right shows the FWHM of the instrumental broadening for the H_2 profile.

In Figure 2, the SiO line profile at the driving source shows flow velocities slower than the H_2 emission at NK 1 and SK 1, the brightest H_2 features in the beam. To investigate this in detail, we averaged the H_2 profiles from NK 1 and SK 1, and plot the results in Figure 4 together with the SiO profile at the driving source. In Figure 4 the velocity centroid is located at the systemic velocity for both SiO and H_2 emission. The SiO profile exhibits two marginal peaks at positive and negative velocities, and these match well with the peak velocity of NK 1 and SK 1, respectively. The FWHM of the H_2 profile is 32 km s^{-1} , broader than SiO ($\sim 20\text{ km s}^{-1}$), although again the difference is attributed to the instrumental broadening of the former profile. We thus conclude that the SiO emission observed towards the driving source is associated with these H_2 knots.

Gibb et al. (2004) observed the SiO $J=5-4$ emission (217.1 GHz) at the driving source and 20'' south using the JCMT, which provides the same beam size as the SiO $J=8-7$ observations at ASTE. The $J=5-4$ profile observed

¹ 0.8 ± 0.3 and $< 0.3\text{ K km s}^{-1}$ for 40'' and 60'' north, respectively, assuming the same line profile as 20'' north; 0.6 ± 0.2 and $< 0.3\text{ K km s}^{-1}$ for 40'' and 60'' south, respectively, assuming the same line profile as 20'' south.

at the driving source is markedly different from the $J=8-7$ profile: the JCMT observations show a blueshifted component peaking at -6 km s^{-1} , and a possible redshifted component peaking close to 28 km s^{-1} . However, the $J=5-4$ and $J=8-7$ line profiles do resemble each other at $20''$ south. Using the $J=5-4$ integrated intensity of $2(\pm 0.6) \text{ K km s}^{-1}$, we derive the $5-4/8-7$ intensity ratio of ~ 1 . Performing comparisons with model calculations by Nisini et al. (2002), we derive a molecular hydrogen number density of $10^6\text{--}10^7 \text{ cm}^{-3}$ assuming a temperature $T=100\text{--}1000 \text{ K}$. This value is $10\text{--}100$ times larger than that obtained by Gibb et al. (2004) using the $2-1/5-4$ intensity ratio ($n_{\text{H}_2} \sim 10^5 \text{ cm}^{-3}$). The discrepancies between our results and those of Gibb et al. (2004) would be attributed to the fact that the upper transitions have higher critical densities (1×10^6 , 2×10^7 and $1 \times 10^8 \text{ cm}^{-3}$ at $T=100 \text{ K}$ for the $J=2-1$, $5-4$ and $8-7$ transitions, respectively).

3. Discussion

Millimeter/sub-millimeter SiO emission has been observed towards a number of molecular outflows for the last decade. Studies to date have shown that the emission originates from the regions with a temperature $T > 100 \text{ K}$ and a molecular hydrogen density $n_{\text{H}_2} > 10^5 \text{ cm}^{-3}$ (see e.g., Codella et al. 1999; Nisini et al. 2002, 2005; Gibb et al. 2004), both much higher than the regions associated with mm CO emission. The abundance of gas-phase SiO in these regions is estimated to be 10^{-11} to 10^{-6} , significantly higher than that of quiescent clouds ($< 10^{-12}$, Ziurys, Friberg & Irvine 1989). This supports the theories, which predict that shocks release silicon-bearing molecules from dust to the gas, allowing bright SiO emission to be observed towards molecular outflows (Schilke et al. 1997; Caselli et al. 1997; Pineau des Forêts et al. 1997).

Chandler & Richer (2001), Hirano et al. (2006) and Palau et al. (2006) conducted high-resolution observations of SiO $J=1-0$, $5-4$ and $8-7$ lines, respectively, towards HH 211. Performing comparisons with the H_2 $1-0 \text{ S}(1)$ image, these authors show that the SiO emission is associated with the collimated jet. Our results for HH 212 show that the kinematics of the SiO emission closely resemble the near-infrared H_2 emission associated with the collimated jet, agreeing with this picture. Since the SiO emission shows nearly the same velocity as the H_2 emission, it is likely that the emission is associated with the ejecta of the collimated jet, in particular with its internal working surfaces. This contrasts with millimeter CO emission, which is markedly slower than the SiO and H_2 emission and probably originates from gas entrained by the jet (Lee et al. 2000), or limb-brightened shells surrounding the H_2 jet (Lee et al. 2006).

While the observed kinematics of the SiO $J=8-7$ emission match well with the H_2 $1-0 \text{ S}(1)$ emission, their intensity distributions markedly differ with each other due to different excitation conditions. Indeed, the shock-excited H_2 $1-0 \text{ S}(1)$ emission originates from regions with a temperature of $\sim 2 \times 10^3 \text{ K}$ (see, e.g., Eisloffel et al. 2000;

Takami et al. 2006), while the SiO emission presumably originates from regions with a much lower temperature due to its low upper energy level ($E_u/k = 75 \text{ K}$ for $J=8-7$). In addition, the critical density of H_2 $1-0 \text{ S}(1)$ is $\sim 10^6 \text{ cm}^{-3}$ for $\text{H}_2\text{--H}_2$ collision, while that of SiO $J=8-7$ is ~ 100 times larger ($1 \times 10^8 \text{ cm}^{-3}$). The enhancement of the $J=8-7$ emission within $1'$ of the driving source is attributed to the density gradient in the jet. The same trend of the SiO $J=8-7$ intensity distribution is also observed in HH 211 by Palau et al. (2006): these authors measured $5-4/8-7$ ratios along the jet, revealing that the gas density is higher near the driving source.

Due to its high critical density, the SiO $J=8-7$ line has the potential to probe the jet/wind launching regions through interferometric observations in the future. However, the emission has not been detected even towards SVS 13 and L1551-IRS 5, which exhibit a bright molecular-hydrogen-emission-line (MHEL) region within a few second of the driving source (Davis et al. 2001, 2002, 2006; Takami et al. 2006). This could be due to the small angular scale of the emission region, and so beam dilution effects, or to the high temperature. Alternatively, the gas density and/or SiO abundance may be too low in these less embedded, more evolved Class I sources. Observations with a higher angular resolution or better signal-to-noise would allow for investigating this in detail.

We acknowledge the ASTE team for their excellent support. We thank Dr. Hirano for useful discussion. The narrow-band images of the H_2 $1-0 \text{ S}(1)$ emission have been obtained through the ESO archive operated by European Southern Observatory. This research has been made use of the Simbad database operated at CDS, Strasbourg, France, and the NASA's Astrophysics Data System Abstract Service.

References

- Bacciotti, F., Mundt, R., Ray, T. P., Eisloffel, J., Solf, J., & Camezind, M. 2000, *ApJL*, 537, L49
- Caselli, P., Hartquist, T. W., & Havnes, O. 1997, *A&A*, 322, 296
- Chandler, C. J., & Richer, J. S. 2001, *ApJ*, 555, 139
- Claussen, M. J., Marvel, K. B., Wootten, A., & Wilking, B. A. 1998, *ApJL*, 507, L79
- Codella, C., Bachiller, R., & Reipurth, B. 1999, *A&A*, 343, 585
- Coffey, D., Bacciotti, F., Woitas, J., Ray, T. P., & Eisloffel, J. 2004, *ApJ*, 604, 758
- Davis, C. J., Berndsen, A., Smith, M. D., Chrysostomou, A., & Hobson, J. 2000, *MNRAS*, 314, 241
- Davis, C. J., Mundt, R., Eisloffel, J., & Ray, T. P. 1995, *AJ*, 110, 766
- Davis, C. J., Nisini, B., Takami, M., Pyo, T.S., Smith, H.D., Whelan, E., Ray, T. P., & Chrysostomou, A. 2006, *ApJ*, 639, 969
- Davis, C. J., Ray, T. P., Desroches, L., & Aspin, C. 2001, *MNRAS*, 326, 524
- Davis, C. J., Stern, L., Ray, T. P., & Chrysostomou, A. 2002, *A&A*, 382, 1021

- Eisloffel, J., Smith, M. D., & Davis, C. J. 2000, *A&A*, 359, 1147
- Ezawa, H., Kawabe, R., Kohno, K., & Yamamoto, S. 2004, *Proc. SPIE*, 5489, 763
- Gibb, A. G., Richer, J. S., Chandler, C. J., & Davis, C. J. 2004, *ApJ*, 603, 198
- Hirano, N., Liu, S.-Y., Shang, H., Ho, P. T. P., Huang, H.-C., Kuan, Y.-J., MacCaughrean, M. J., & Zhang, Q. 2006, *ApJ*, 636, L141
- Hirano, N., Mikami, H., Umemoto, T., Yamamoto, S., & Taniguchi, Y. 2001, *ApJ*, 547, 899
- Königl, A., & Pudritz, R. E. 2000, *Protostars and Planets IV*, 759
- Lee, C.-F., Ho, P. T. P., Beuther, H., Bourke, T. L., Zhang, Q., Hirano, N., & Shang, H. 2006, *ApJ*, accepted
- Lee, C.-F., Mundy, L. G., Reipurth, B., Ostriker, E. C., & Stone, J. M. 2000, *ApJ*, 542, 925
- Mikami, H., Umemoto, T., Yamamoto, S., & Saito, S. 1992, *ApJL*, 392, L87
- Nisini, B., Codella, C., Giannini, T., Bachiller, R., Santiago Garcia, J., & Richer, J. S. 2005, *The Dusty and Molecular Universe: A Prelude to Herschel and ALMA*, 397
- Nisini, B., Codella, C., Giannini, T., & Richer, J. S. 2002, *A&A*, 395, L25
- Palau, A., Ho, P. T. P., Zhang, Q., Estalella, R., Hirano, N., Shang, H., Lee, C.-F., Bourke, T. L., Beuther, H., & Kuan, Y.-J. 2006, *ApJ*, 636, L137
- Pineau des Forêts, G., Flower, D. R., & Chieze, J.-P. 1997, *IAU Symp. 182: Herbig-Haro Flows and the Birth of Stars*, 182, 199
- Schilke, P., Groesbeck, T. D., Blake, G. A., & Phillips, T. G. 1997, *ApJS*, 108, 301
- Schilke, P., Walmsley, C. M., Pineau des Forêts, G., & Flower, D. R. 1997, *A&A*, 321, 293
- Shu, F. H., Najita, J. R., Shang, H., & Li, Z.-Y. 2000, *Protostars and Planets IV*, 789
- Takami, M., Chrysostomou, A., Ray, T. P., Davis, C., Dent, W. R. F., Bailey, J., Tamura, M., Terada, H., & Pyo, T.-S. 2006, *ApJ*, 641, in press
- Wiseman, J., Wootten, A., Zinnecker, H., & McCaughrean, M. 2001, *ApJL*, 550, L87
- Woitak, J., Bacciotti, F., Ray, T. P., Marconi, A., Coffey, D., & Eisloffel, J. 2005, *A&A*, 432, 149
- Zinnecker, H., McCaughrean, M. J., & Rayner, J. T. 1998, *Nature*, 394, 862
- Ziurys, L. M., Friberg, P., & Irvine, W. M. 1989, *ApJ*, 343, 201